Scientific Research Publishing

Atmospheric and Climate Sciences, 2026, 16(3), 530-556
https://www.scirp.org/journal/acs
ISSN Online: 2160-0422
ISSN Print: 2160-0414

Analysis of the Impact of Emissivity and Albedo on Urban Mean Radiative Temperature

Hervé Pron[1,2], Abdelilah Zyane[1]

[1]University of Reims Champagne Ardenne (URCA), Reims, France
[2]Institut de Thermique, Mécanique et Matériaux, EA 7548/Equipe Thermique-Energétique, Campus du Moulin de la Housse, Reims, France
Email: herve.pron@univ-reims.fr, abdelilah.zyane@univ-reims.fr

How to cite this paper: Pron, H. and Zyane, A. (2026) Analysis of the Impact of Emissivity and Albedo on Urban Mean Radiative Temperature. *Atmospheric and Climate Sciences*, **16**, 530-556.
https://doi.org/10.4236/acs.2026.163027

Received: April 1, 2026
Accepted: May 16, 2026
Published: May 19, 2026

Copyright © 2026 by author(s) and Scientific Research Publishing Inc.
This work is licensed under the Creative Commons Attribution International License (CC BY 4.0).
http://creativecommons.org/licenses/by/4.0/

Open Access

Abstract

This study investigates the impact of urban surface albedo and emissivity on Mean Radiant Temperature (MRT), a key parameter for assessing thermal comfort and urban heat island (UHI) dynamics. Results show that MRT generally follows the diurnal cycle of air temperature, with notable deviations in highly exposed areas, particularly on horizontal surfaces, which are more sensitive due to their orientation, thermal capacity, and roughness. High-albedo scenarios effectively reduce daytime MRT and summer heat stress but may also enhance nocturnal radiative cooling. The influence of emissivity is more subtle, as most urban materials already exhibit high values, yet variations can still affect longwave exchanges, especially at night. Intermediate albedo-emissivity configurations provide a more balanced performance across seasons by maintaining moderate MRT levels both day and night. Findings further indicate that horizontal surfaces exert a stronger control on MRT than vertical ones under open-sky conditions, though facades can become dominant in dense urban canyons due to radiative trapping. Additionally, integrating urban vegetation—through evapotranspiration and shading—proves highly effective in lowering MRT and mitigating UHI. Optimizing the radiative properties of urban surfaces, combined with green infrastructure, can improve outdoor thermal comfort, reduce cooling energy demand, and indirectly contribute to lowering greenhouse gas (GHG) emissions. These results provide operational insights for incorporating MRT into energy-climate planning and guiding urban transition strategies towards more resilient and sustainable cities.

Keywords

Urban Heat Island, Urban Dynamic Thermal Simulation, Urban Energy Transition, Energy-Climate Planning, Climate Change

1. Introduction

The energy transition represents a major challenge for ensuring a sustainable and resilient future. In this context, promoting strategies to mitigate the effects of global warming at the urban scale is essential. According to the Intergovernmental Panel on Climate Change (IPCC) [1], global temperatures have already increased by approximately 1.5˚C relative to pre-industrial levels, accompanied by rising greenhouse gas (GHG) emissions (IPCC) [2]. Rapid urbanization further exacerbates these challenges, as the global population is projected to reach 10 billion by 2050, with nearly 68% living in urban areas [3]. This urban expansion significantly alters microclimatic conditions, increasing surface and air temperatures while reducing convective heat exchange and negatively affecting urban energy balances [4]. The complexity of these urban climate processes has been highlighted through the development of urban climate classification systems such as Local Climate Zones (LCZ), which link urban morphology, land cover, and thermal behavior [5].

Radiative parameters, particularly albedo and emissivity, strongly influence mean radiant temperature (MRT) and outdoor thermal comfort. Deterioration of thermal comfort increases health risks, intensifies surface heating, raises cooling energy demand, and complicates efforts to reduce GHG emissions [6]. Urban morphology further affects radiative exchanges through shading, three-dimensional reflections, and the physical properties of construction materials [7]. The albedo of the urban canopy—encompassing both horizontal and vertical surfaces—is therefore a key factor in evaluating radiative heat fluxes exchanged with the atmosphere.

Previous research has examined the impact of urban design on urban heat islands. [8] highlighted how urban geometry, morphological parameters, and building envelope characteristics influence both energy efficiency and outdoor thermal comfort using optimization frameworks such as Grasshopper plugins (Ladybug and Eddy3D). Other studies considered energy infrastructure, spatial characteristics, and additional morphological aspects [9]. Spatio-temporal analyses of external comfort temperature (ECT) revealed that factors such as wind and solar radiation significantly influence thermal comfort variations throughout the day [10]. Similarly, the role of urban vegetation in mitigating heat islands was emphasized by [11], while studies on urban thermal inertia highlighted the importance of anthropogenic heat and circulation dynamics.

Despite these advances, the combined influence of radiative surface properties particularly albedo and emissivity on the urban energy balance and mean radiant temperature remains insufficiently explored at the scale of the urban canopy. While many studies have addressed the effects of urban morphology, vegetation, and energy infrastructures on urban heat island intensity and outdoor thermal comfort, fewer investigations have specifically focused on the radiative properties of commonly used urban materials. Yet, these parameters strongly influence the reflection, absorption, and re-emission of solar and thermal radiation, which directly affect MRT and the thermal perception of outdoor spaces [12]. In this con-

text, the present study provides a systematic analysis of the influence of albedo and emissivity on urban thermal conditions.

Albedo, representing the surface's ability to reflect solar radiation, varies across ultraviolet, visible, and near-infrared spectra. High-albedo surfaces reflect most solar radiation and enhance cooling, whereas low-albedo surfaces absorb radiation and contribute to warming. Emissivity is particularly relevant in the thermal infrared range (3 - 5 μm for high temperatures, 8 - 14 μm for ambient conditions) and affects energy re-emission from urban materials. Several simulation scenarios were therefore developed to identify optimal values for these parameters, aiming to mitigate the negative impacts of commonly used urban materials and enhance thermal comfort at the urban scale.

To address this gap, this study examines how variations in albedo and emissivity affect mean radiant temperature (MRT) and the urban energy balance using UMEP/SOLWEIG. It analyzes upward and downward shortwave (K) and longwave (L) radiation components, providing a concise contribution beyond prior studies focused mainly on urban morphology and vegetation.

2. Methodology

The framework developed in this study proposes a step-by-step methodology to optimize the albedo and radiative emissivity of urban surfaces, considering the diverse material properties present in the built environment. This approach is based on a dynamic thermal simulation of mean radiative temperature, using the UMEP-SOLWEIG model integrated within QGIS. The computational model was applied to the city of Reims, with spatial data acquired through LIDAR technology.

The analysis framework consists of three main stages, as illustrated "in **Figure 1**". The first stage involves the mapping of 2D and 3D spatial geometry through the extraction of raw geospatial data. The second stage focuses on the development of a comprehensive database of material properties, integration of meteorological data, and satellite-derived observations of albedo and emissivity values to construct relevant simulation scenarios. The third and final stage entails the simulation of mean radiative temperature using the UMEP-SOLWEIG tool within QGIS. This enables the evaluation of thermal comfort conditions at the urban scale and the subsequent assessment of the urban heat island effect.

Study zone: City of Reims, France

Reims is a commune located in the Marne department (department 51) "as shown in **Figure 2**". below, in Champagne-Ardenne region of northeastern France. As of 2020, the city had an estimated population of approximately 185,034 residents, compared to 183,113 in 2016. With a total area of 49.41 km2, this corresponds to a population density of around 3745 inhabitants per square kilometer.

It has been observed that the temperature in the city of Reims has continuously increased over time, "as shown in **Figure 3** below". This highlights the importance of focusing on improving urban outdoor thermal comfort by optimizing the mean radiative temperature.

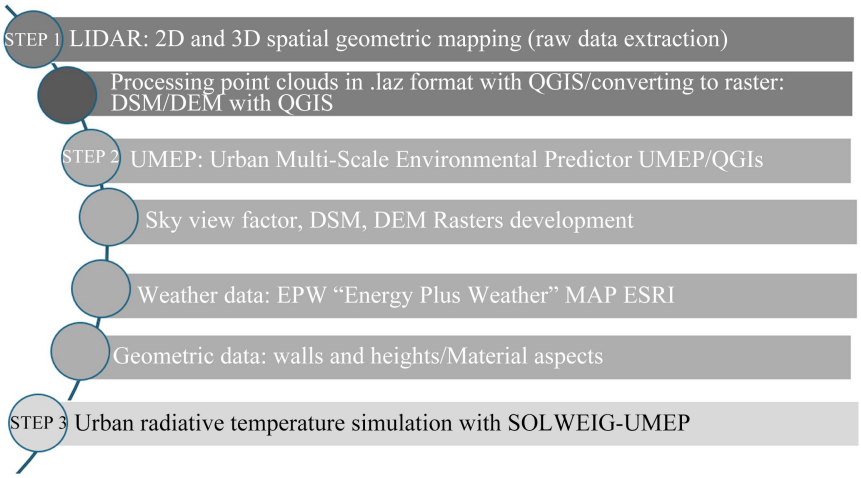

Figure 1. Urban radiative temperature simulation steps.

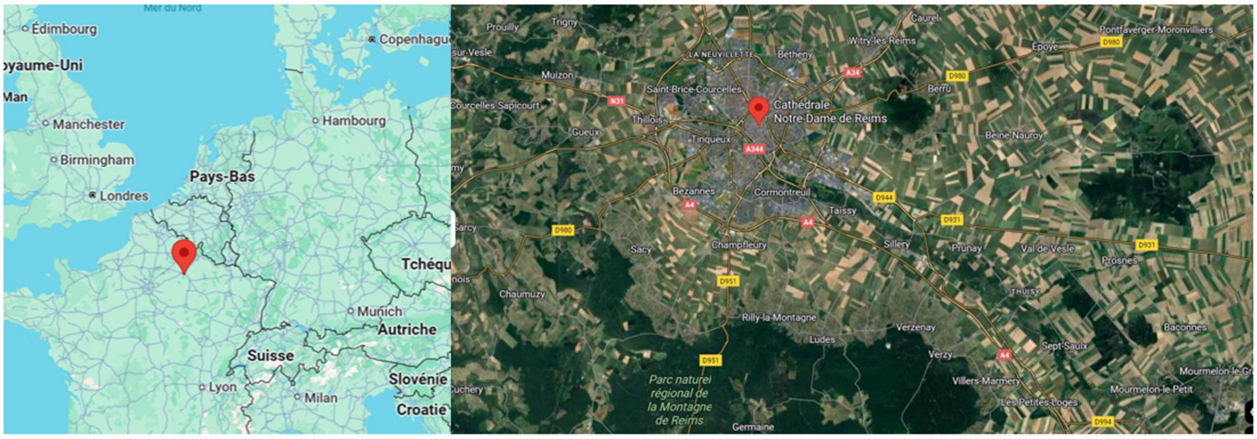

Figure 2. Geographical location of the city of Reims France.

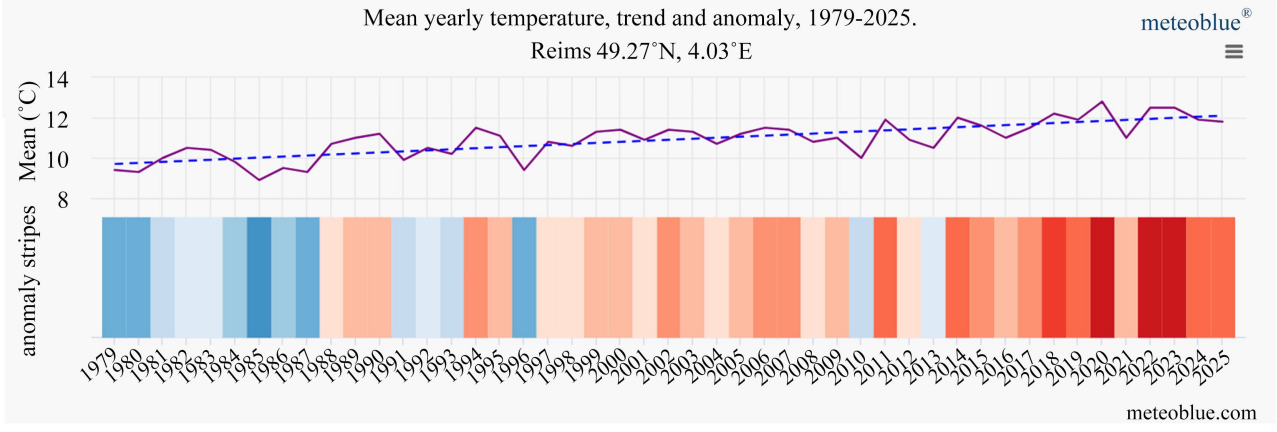

Figure 3. Mean yearly air temperature evolution in the city of Reims-1979-2023 source Météo France-meteoblue.

The study area is centered on Cathédrale Notre-Dame de Reims, along a main axis following Avenue de la Paix and extending across the city center. It is defined by a radius of approximately 950 m (corresponding to a diameter of about 1.9

km), covering an area of roughly 2.8 km^2. Mean radiant temperature (MRT) was measured at a standard height of 1.8 m above ground, representative of human perception in outdoor environments.

In this study, a spatial resolution of 1 m was adopted with the use of a resolution of 0.5 m for the validation of the calculation model for small study areas. The Raster maps are based on the LiDAR HD data provided by the IGN (average density of 10 to 20 points/m^2), the rasters were generated from the raw data. LAZ tiles delivered by IGN.

Between 1979 and 2023, the annual mean air temperature exhibits a clearly increasing trend, rising from approximately 9.5˚C to over 12.5˚C. Despite some year-to-year variability, the overall curve reflects continuous warming. This trend is further emphasized by the visualization of "anomaly stripes": colder years (in blue) dominate until the mid-1990s, while recent years particularly after 2010 are mostly warm (in dark red). The graph thus provides a clear and visual representation of the progression of climate warming over the past four decades.

2.1. Step 1: Data Extraction Using 2D and 3D HD LiDAR Geometric Mapping

LiDAR technology was utilized for terrain mapping and the development of digital elevation models, enabling the generation of high-resolution 3D representations of the city of Reims. These models are essential for conducting radiative thermal analyses of urban heat islands, particularly through the assessment of MRT.

LiDAR an acronym for Light Detection and Ranging is an optical remote sensing technique that uses laser pulses to densely scan the Earth's surface, producing highly accurate x, y, and z coordinates. This technology allows for the detailed reconstruction of both terrain and above-ground features.

As part of the national LiDAR HD program, the French National Institute of Geographic and Forestry Information (IGN) is responsible for producing and disseminating comprehensive 3D mapping of both ground and surface features across France using LiDAR data. The datasets provided include calibrated point clouds (both raw and classified), as well as 3D digital models such as Digital Terrain Models (DTM), Digital Surface Models (DSM), and Digital Height Models (DHM).

For this study, raw LiDAR HD data "in **Figure 4** below" for the city of Reims was extracted. Each x, y, z point in the dataset contains additional metadata that enriches the spatial analysis. The map below illustrates the various available LiDAR data tiles across France, allowing users to download point clouds corresponding to their area of interest.

The tiles are represented by HD LiDAR point clouds, which are subsequently converted into raster format using "in **Figure 5**".

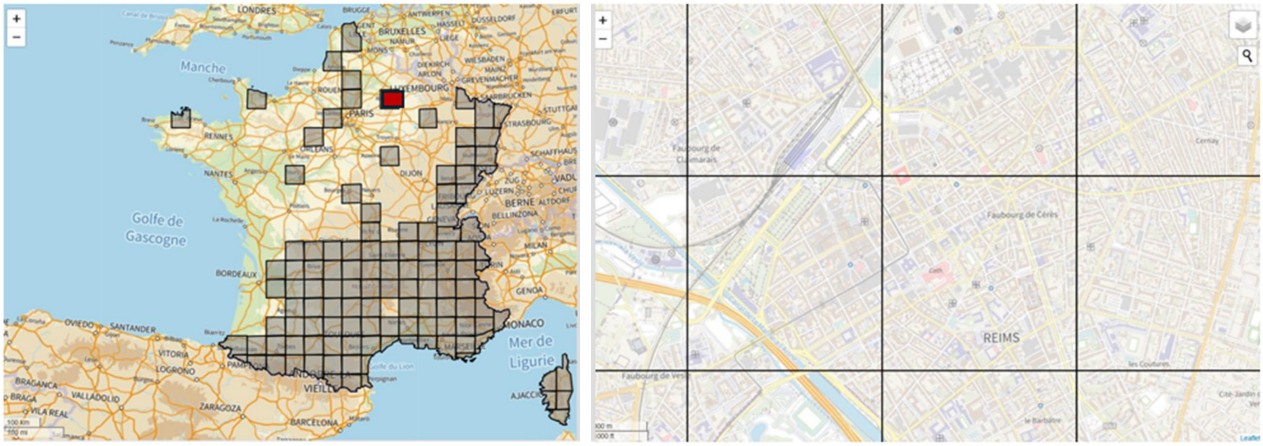

(a) (b)

Figure 4. HD LIDAR data tiles. (a) The different Lidar tiles in France, (b) The different Reims tiles used as raw data for the calculation.

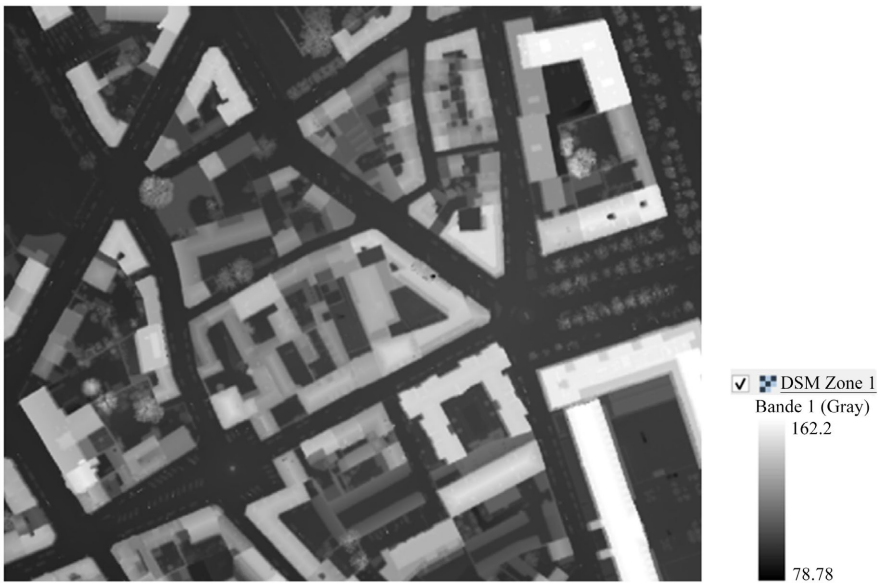

Figure 5. Map illustrating the digital surface model (DSM) of the study area.

Raster maps are used to represent various elevation-related geospatial datasets, including the Digital Elevation Model (DEM), Digital Surface Model (DSM), Digital Terrain Model (DTM), and the Normalized Digital Surface Model (NDSM). These four components are essential for accurately characterizing urban morphology, which contain classified LiDAR point clouds subsequently interpolated to produce elevation models. Georeferencing within QGIS is a crucial step in aligning raster images to ensure consistency and reliability in subsequent simulations.

The Sky View Factor (SVF) plugin is employed to calculate the SVF for each pixel (1 m × 1 m), based on DSM data that captures both ground and built surfaces. The Sky View Factor is the ratio of radiation received (or emitted) by a flat surface to the radiation that would be received (or emitted) from the entire hem-

ispherical sky dome [13]. It is a dimensionless index ranging from 0 to 1, where 0 represents fully obstructed environments and 1 indicates completely open spaces. The methodology for generating SVF values follows the approach outlined by [14].

The wall height and aspect pre-processor are employed to detect wall pixels and estimate their height using digital surface models (DSMs) of the terrain and built structures. This process involves the application of a filtering technique described by [15]. Wall aspect is determined through a specialized linear filter originally proposed and subsequently refined by [15].

2.2. Step 2

The process entails the retrieval of meteorological data from EnergyPlus Weather (EPW) files, followed by the analysis of surface albedo and emissivity values derived from satellite observations.

Meteorological data from EnergyPlus Weather (EPW) files, combined with satellite-derived datasets provided by the Environmental Systems Research Institute (ESRI), were employed to integrate atmospheric and surface information into the calculation of mean radiant temperature. This integration enables a more accurate representation of radiative thermal dynamics, which is essential for the analysis of urban heat island effects.

Figure 6 below illustrates the geolocation of the different stations with IWEC (International Weather for Energy Calculations) meteorological data, which are based on 18 to 25 years of historical measurements and cover over 2000 sites worldwide. It also shows the TMYx (Typical Meteorological Year-extended) files used in our calculations, which rely on more recent and extensive datasets, providing a better representation of current climatic conditions for energy simulation and thermal comfort assessment.

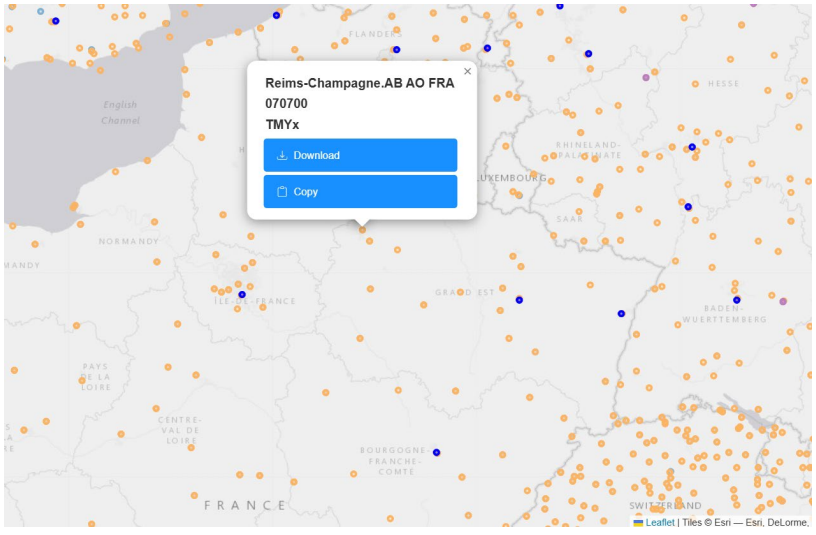

Figure 6. Meteorological Data EPW: source EPW Map (ladybug.tools), with the various orange TMYx (and blue IWEC (International Weather for Energy Calculations) dot stations.

In the case of the city center, the raw TMYx meteorological data were adjusted to better represent the urban microclimate. The meteorological station used to generate the TMYx files ("Reims-Champagne 070700") is located at Reims airport. To account for urban conditions, a temperature increment characteristic of the nocturnal urban heat island was applied: the air temperature was increased by 1.5˚C. Wind speed values were adjusted based on surface roughness and building obstructions, using a logarithmic profile to scale measurements from the airport (~10 m above ground) down to the urban pedestrian level (~2 m). These adjustments were applied across the different study zones in the city center of Reims and were validated through infrared measurements, in order to better capture actual city-center conditions.

The calculation model allowed us to simulate the radiative exchanges between urban surfaces and the human body, taking into account both shortwave (solar) and longwave (thermal) radiation. In this context, the reflections and spectral emissivity of materials play a crucial role in the spatial distribution of the energy flux received and emitted.

In the solar shortwave spectrum (approximately 0.3 - 3 μm), which encompasses the visible (0.4 - 0.7 μm) and near-infrared NIR and short-wave infrared SWIR (0.7 - 3 μm) ranges, the SOLWEIG model uses predefined surface reflectance (albedo) values to estimate the proportions of direct, diffuse, and reflected solar radiation reaching the individual. In radiative modelling, K and L denote the two main components of radiation: K refers to shortwave solar radiation (0.3 - 3 μm), including direct, diffuse, and reflected solar fluxes, while L corresponds to longwave radiation (4 - 100 μm), emitted by the atmosphere and surrounding surfaces. Together, these two components determine the total radiative load governing surface energy balance and human thermal comfort.

In the thermal infrared range (4 - 100 μm), the Stefan-Boltzmann law governs the radiative emission of surfaces, weighted by their emissivity (ε), resulting in longwave radiation emissions. The human body, considered in the model as a nearly perfect absorber ($\varepsilon \approx 0.97$), thermally interacts with these surfaces through infrared radiation exchanges, directly influencing the MRT.

The calculation model also incorporates the geometric effect of the Sky View Factor (SVF) and the three-dimensional distribution of obstacles to determine the visible portion of the sky, dynamic shading, and multiple reflections between surfaces. Thus, the combined consideration of spectral reflectance, thermal emissivity, and urban morphology allows for accurate modeling of local radiative balances.

The observation and satellite-based modeling of albedo values in the visible and near-infrared spectra will facilitate the identification of these values, which can then be integrated into various optimization scenarios.

Figure 7 below illustrate White-Sky Albedo (WSA) maps for a gray body: visible range (WSA_vis) on the left and near-infrared range (WSA_nir) on the right. The maps illustrate spatial variations in surface reflectivity over the selected region

(France and surrounding areas) for the period from 14 to 29 July 2023. Higher albedo values (lighter colors) indicate more reflective surfaces, while darker tones correspond to lower reflectivity. The WSA_nir values are slightly higher than those in the visible range, reflecting the stronger reflectance of most natural and urban materials in the near-infrared spectrum under the gray-body assumption.

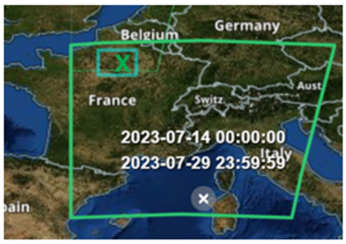

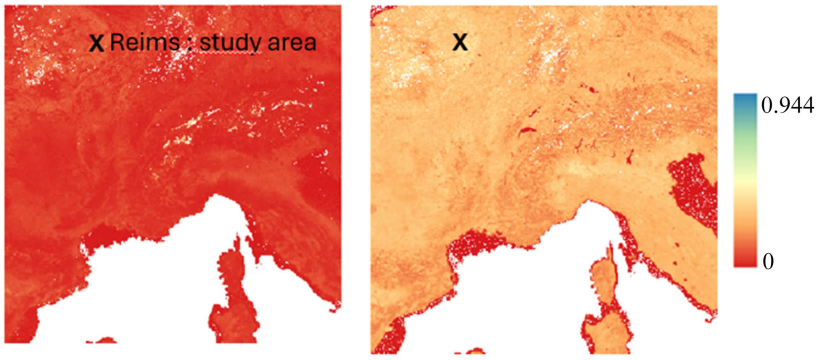

Bande 1: Albedo_WSA_vis (Gray) Bande 1: Albedo_WSA_nir (Gray)

Sources: MODIS/Terra+Aqua BRDF/Albedo Albedo Daily L3 Global-500 m V061|Earthdata Search (https://search.earthdata.nasa.gov/).

Figure 7. Albedo observation map WSA "White Sky Albedo" visible "Vis" on left side and Albedo WSA nir "Near Infrared" in the right side.

2.3. Step 3

Approach and methodology for simulating MRT are implemented using UMEP (Urban Multi-scale Environmental Predictor) and the SOLWEIG (Solar and LongWave Environmental Irradiance Geometry) model.

UMEP is an extension module for QGIS, a Geographic Information System (GIS) software, which enhanced by UMEP, enables advanced geospatial analysis. This integration is particularly useful for studying outdoor thermal comfort and climate change mitigation.

SOLWEIG is employed to estimate spatial variations in 3D radiation fluxes and mean radiant temperature (MRT). Shortwave and longwave radiation fluxes from six directions are calculated separately to derive the MRT. The model requires a limited set of inputs, including direct, diffuse, and global shortwave radiation, air temperature, relative humidity, urban geometry, and geographical data (latitude, longitude, and altitude). Additionally, information on vegetation and its cover is incorporated to improve the estimation of MRT.

The calculation method utilizes longwave sky irradiation as isotropic, estimating it from sky view factors (SVF) and global emissivity [16]. However, in line with the (SRA) [17] for diffuse sky irradiance, partitioning the sky vault is recommended to achieve more realistic results for longwave sky radiation.

The integration of the Sky View Factor (SVF) is crucial for capturing urban microclimates, as it regulates the balance between direct and diffuse visible radiation, and diffuse longwave radiation. Low SVF in dense canyons reduces direct

solar input but enhances radiative trapping, while high SVF increases overall exposure. The solar elevation angle further amplifies these effects, making SVF a key parameter for explaining spatial variability in MRT.

Celestial radiation is composed of three main components: direct shortwave irradiation, diffuse shortwave irradiation, and longwave irradiation. The mean radiant flux used in SOLWEIG is based on the equation developed by [18], which divides the observed global radiation into direct and diffuse shortwaves. The observed global radiation in both direct and diffuse shortwaves is described as follows, with the mean radiant flux (S_{str}):

$$S_{str} = \alpha_k \left[0.28 \cdot K_{dir,side} \cdot f(\theta_s) + 0.06\left(K_{up} + K_{down}\right) + 0.88 K_{dif,side} \right] + \varepsilon_p \left[0.88 L_{side,average} + 0.06\left(L_{up} + L_{down}\right) \right] \quad (1)$$

α_k : is the absorption coefficient for short-wave radiation (standard value 0.7)

ε_p : the average emissivity of the human body of the human body (equal to the long-wave absorption coefficient according to Kirchoff's law, with a standard value of 0.97).

$K_{dir,side}$: is the horizontal component of direct radiation normal to the surface of the cylinder body.

$K_{dif,side}$: the corresponding diffuse radiation.

$L_{side,average}$: average flux of the four cardinal points of the long-wave sensors. The coefficients 0.28, 0.06 and 0.88 are cylinder form factors. Vertical section area, top/bottom, and bole area.

K_{up} : outgoing radiation.

L_{up} : short-wave radiation emitted from above.

K_{down} : short-wave radiation from high output.

L_{down} : broad-wavelength radiation emitted from above.

$f(\theta_s)$: solar ponderation factor: $f(\theta_s) = \cos(i) = \sin(\theta_s) \cdot \cos(\Delta\phi)$.

θ_s : solar elevation (in radians or degrees).

i : angle of incidence on the lateral surface.

$\Delta\phi$: azimuth difference between the sun and the normal to the wall.

The following values correspond to:

0.28: vertical section area, this corresponds to the contribution of the cylinder's lateral surface, representing the portion of the surface exposed vertically.

0.06: top and bottom surfaces, this coefficient represents the combined contribution of the cylinder's top and bottom surfaces.

0.88: bole area (trunk area), the "bole" refers to the main trunk of the cylinder. This coefficient indicates the proportion of the total surface attributed to the trunk.

In SOLWEIG, [15] expression is used to estimate global clear-sky emissivity (ε_{sky}):

$$\varepsilon_{\text{sky}} = 1 - \left(1 + 46.5\frac{e_a}{T_a}\right) \cdot \exp\left(-\left(1.2 + 3.0 \cdot 46.5\frac{e_a}{T_a}\right)^{0.5}\right) \quad (2)$$

where T_a is the air temperature at standard height (2 m) and e_a is the actual vapor pressure in hPa calculated from observations of relative humidity at standard height, where e_a in SOLWEIG is estimated from T_a and relative humidity (RH):

$$Tmrt = \sqrt[4]{\frac{S_{str}}{\varepsilon_{p-\sigma}}} - 273.15 \tag{3}$$

In the calculation model, the solar elevation angle (θ_s) plays a key role in determining the total shortwave radiation received by urban surfaces and the human body. The total shortwave irradiance is decomposed into three components: direct (K_{dir}), diffuse (K_{dif}), and reflected (S_{str}), according to ($K_{tot} = K_{dir} + K_{dif} + S_{str}$). The direct component is calculated from the solar incidence angle i ($K_{dir} = K_b \cdot \cos(i)$), which depends directly on the solar elevation and surface orientation. As the solar elevation increases, the direct irradiance intensifies, while lower angles enhance shading and increase the relative contribution of diffuse radiation.

The reflected component S_{str}, representing the shortwave radiation reflected from surrounding surfaces, is simplified in SOLWEIG using a constant projection factor ($S_{str} = 0.28 \times K_{dir,side}$), which estimates the average lateral flux reaching the human body. At low solar elevations, lateral reflections are stronger due to increased façade illumination, whereas at higher solar elevations, their contribution decreases. Finally, the solar elevation angle governs both the shading geometry and the visible sky fraction (SVF), thus controlling the spatial distribution of radiative fluxes and the resulting MRT.

Simulation parameters:

Meteorological data, along with raster data containing information on building and ground elevation (DSM) and relative humidity, were sourced from a compiled dataset. Ground cover information, which allows for the differentiation of emissivity, albedo, and surface temperature across various surfaces (e.g., pavement, asphalt, soil, grass), was also included. The MRT is then calculated for a human, modeled as either a box or a cylinder.

The materials considered in the scenarios were selected to represent typical urban surfaces commonly found in the region, including pavements, facades, and ground covers such as asphalt, concrete, brick, roof tiles, glazing, and vegetated surfaces. The selected set also covers a wide range of radiative properties (emissivity and albedo) in order to represent different levels of solar absorption and thermal emission observed in urban environments. This diversity allows the simulations to capture the influence of various material characteristics on radiative exchanges and outdoor thermal conditions under the local climatic context.

Table 1 below illustrates the different calculation parameters, scenarios, calculation and hypothesis:

Table 2 below illustrates the output radiative parameters properties after calculation and simulation of different scenarios:

Table 1. Conditions and hypothesis for calculation and simulation.

Conditions and Hypothesis for calculation		Materials		Fixed input radiative properties				Dynamic input properties			
		Horizontal	Lateral	Ground emissivity	Lateral emissivity	Ground albedo	Lateral albedo	Tair (˚C)	Speed air (m/s)	Precipitation (mm)	RH air %
Scenarios	Reference	Asphalt	Brick	0.93	0.89	0.19	0.23	EPW weather data sources			
	1	Dry soil	Concrete	0.95	0.91	0.2	0.25				
	2	Light-colored concrete	Glazing	0.91	0.87	0.18	0.21				
	3	Dark concrete	Tiles	0.89	0.85	0.17	0.19				
	4	Roof tiles	Metal	0.87	0.83	0.16	0.17	**Atmospheric conditions:** Radiative absorption ratio: SW/LW, Shading SKV: Sky view factor			
	5	Wood	Composite panels	0.85	0.81	0.15	0.15				
	6	Resin	Acrylic paint	0.8	0.79	0.14	0.13				
	7	Lawn	Plant Covering	0.74	0.73	0.11	0.1				
Hypothesis for calculation	**Fixed input radiation parameters**			Average soil and lateral emissivity: wavelength-independent grey body				from 0 to 1			
				Short-wave absorptivity-Long-wave absorptivity				0.7 - 0.95			
				Human surface temperature				34˚C			
				The average emissivity of the human body (equal to the long-wave absorption coefficient according to Kirchhoff's law with a standard value of 0.97, set here at.				0.97			
				Average soil and lateral albedo				from 0.1 to 0.25			

Table 2. Output radiative parameters properties after calculation and simulation of different scenarios.

Results				
Output radiative parameters properties after calculation and simulation of different scenarios				
K_{down} (W/m²)	K_{up} (W/m²)	L_{down} (W/m²)	L_{up} (W/m²)	T_s (˚C)
Incoming direct solar radiation	Reflected solar radiation	Atmospheric longwave radiation	Surface-emitted longwave radiation	Surface temperature
⇩				
Mean radiative temperature MRT (˚C)				

Model Validation:

The MRT was validated through simulations based on infrared measurements of radiative temperature in three areas with distinct morphologies: central Reims

(Zone 1), a natural park (Zone 2), and the semi-urban area of Bétheny (Zone 3). The measurement periods were selected to match the environmental conditions of the two analysis simulation days, winter (January 10, D10) and summer (July 17, D203). Measurements obtained using an infrared camera served as a reference to compare with results from the SOLWEIG model. The differences between measured and simulated temperatures average values are consistent, around 0.3˚C across all zones (Zone 1: 4.1˚C vs 3.8˚C; Zone 2: 1.4˚C vs 1.1˚C; Zone 3: 3.4˚C vs 3.1˚C), confirming the model's accuracy and reliability across different morphologies.

3. Results

1) Study zones:

The calculation models for the MRT simulation were carried out for 4 zones with different characteristics, selected according to the criteria in Table 3 below:

Table 3. Criteria for selecting study areas.

Climate local zone CLZ		Central zone Z1	Natural park zone Z2	Peri-urban zone Z3	Rural zone Z4
Morphology	Ratio surface/typology	high building density 5 floors	high canopy density	medium building density 2 floors	medium canopy density 2 floors
Geometry	Heights	≤20 m	≤25 m	≤8 m	≤8 m
	Density/Occupation	Medium	High	Low	Low
	Orientations	North-south	North-south	North-south	North-south
	Opacity/glazing ratio	Mean/0.3	High/na	Low/na	Low/na
	Inertia	Medium	Low	Low	Low
Material properties	Lateral emissivity	0.91	0.71	0.91	0.71
	Ground emissivity	0.95	0.71	0.85	0.71
	Lateral albedo	0.25	0.2	0.25	0.2
	Ground albedo	0.2	0.11	0.15	0.11
Atmospheric properties	Radiative absorption SW/LW	0.7/0.95***			
	Shading	Integrated according to sky view factor SVF			
	Sky view factor SKV	0.5 - 0.7	<0.4	>0.7	>0.9
	Meteorological data (RH %, Air T…)	EPW meteorological database			

-Surface ratio: Digital surface model (lateral and horizontal).

-Glazed area ratio: 0.3 (30% glazed area).

-Opacity: Degree of light penetration at urban ground level.

-SVF (Sky View Factor): Ratio between the visible portion of the sky hemisphere from the ground and that of an unobstructed hemisphere.

-***Radiative absorption value: Calculated using the non-absorbent atmosphere option.

The different study zones are presented "as follows in Figure 8":

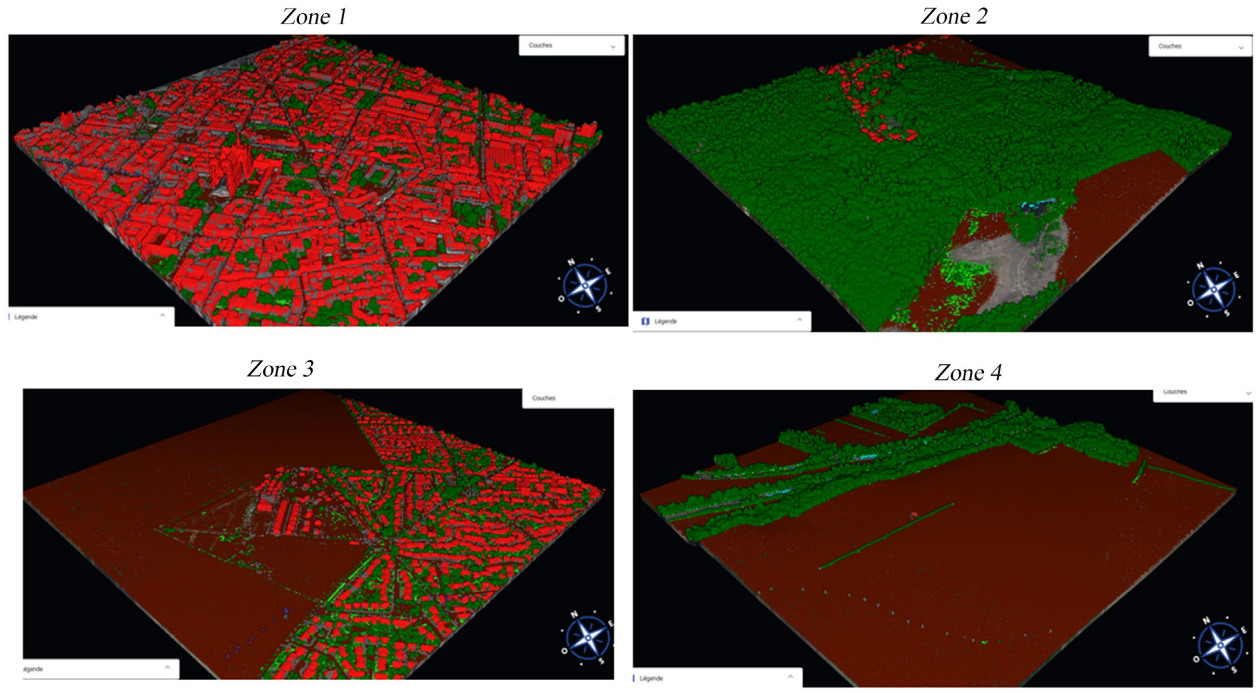

Sources: LiDAR HD|Géoservices (https://diffusion-lidarhd.ign.fr/).

Figure 8. Geographical map of study areas.

To develop the various simulations of mean radiant temperature, Table 3 presents the calculation conditions, distinguishing between variable data specific to each zone and fixed calculation parameters applicable to all zones.

2) Results of mean radiative temperature (MRT) analysis on study zones:

The mean radiant temperature (MRT) calculations, simulated using the UMEP (Urban Multi-scale Environmental Predictor) and SOLWEIG (Solar and Longwave Environmental Irradiance Geometry) models, were conducted for the reference year 2013, spanning 365 days. The simulations utilized an EPW meteorological database, source_EPW Map (ladybug. tools), which was directly integrated into SOLWEIG. To analyze MRT across the study zones over the entire year, simulations were conducted for all days of the year. However, for the purpose of clarity and representation, only two specific days corresponding to the annual extremes were selected for presentation: D10 (January 10) and D203 (July 22), as illustrated in Figure 9 and Figure 10 below.

Figure 9 illustrates the hourly evolution of MRT differences across four areas surrounding Reims (city center, natural park, Bétheny, rural zone). A typical winter thermal pattern is observed: MRT drop sharply during the night, reaching a minimum around 7-8 a.m., then rise again during the day until approximately 3 p.m. In this particular year, winter conditions were exceptionally cold, with air temperature dropping to around −12˚C. Rural areas exhibit the lowest tempera-

tures, especially at night, whereas the city center remains significantly warmer, indicating the presence of an urban heat island effect. This MRT contrast between urban and rural zones highlights the impact of urbanization on local climate conditions, particularly with respect to nocturnal cooling.

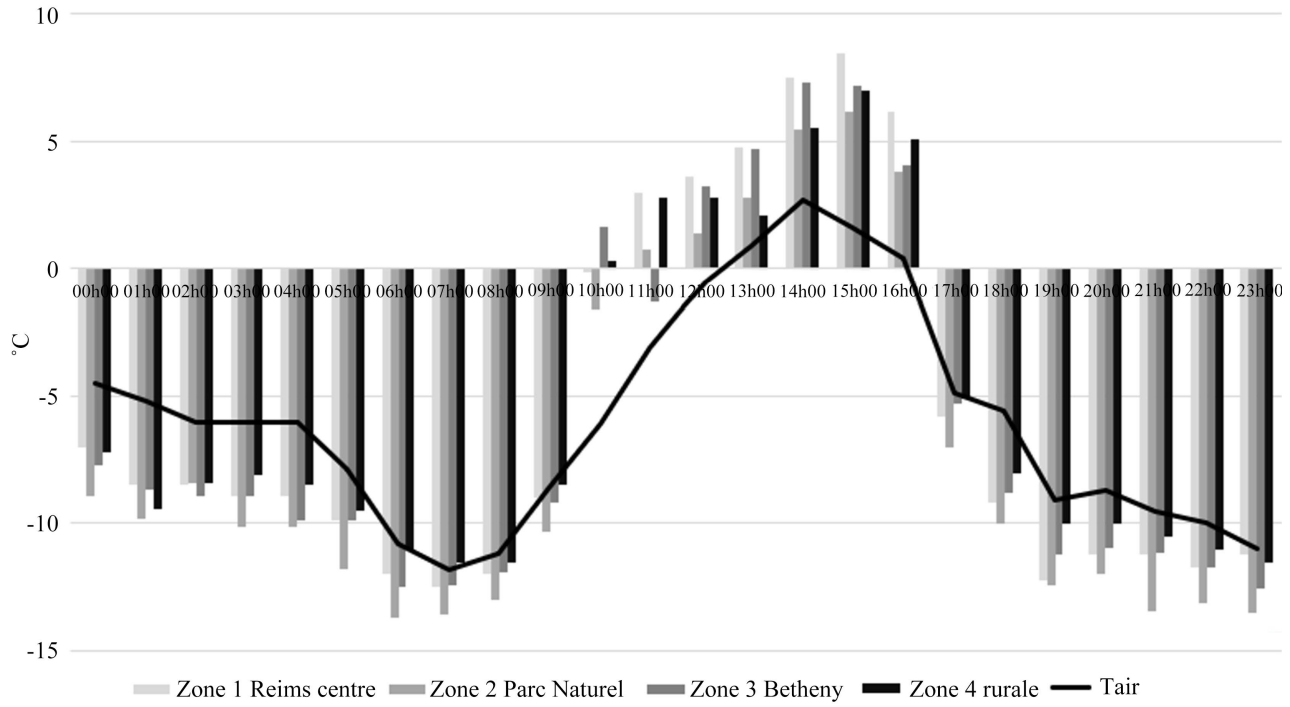

Figure 9. Analysis of the mean radiative temperature of the study areas over 24 hours in January as a function of air temperature.

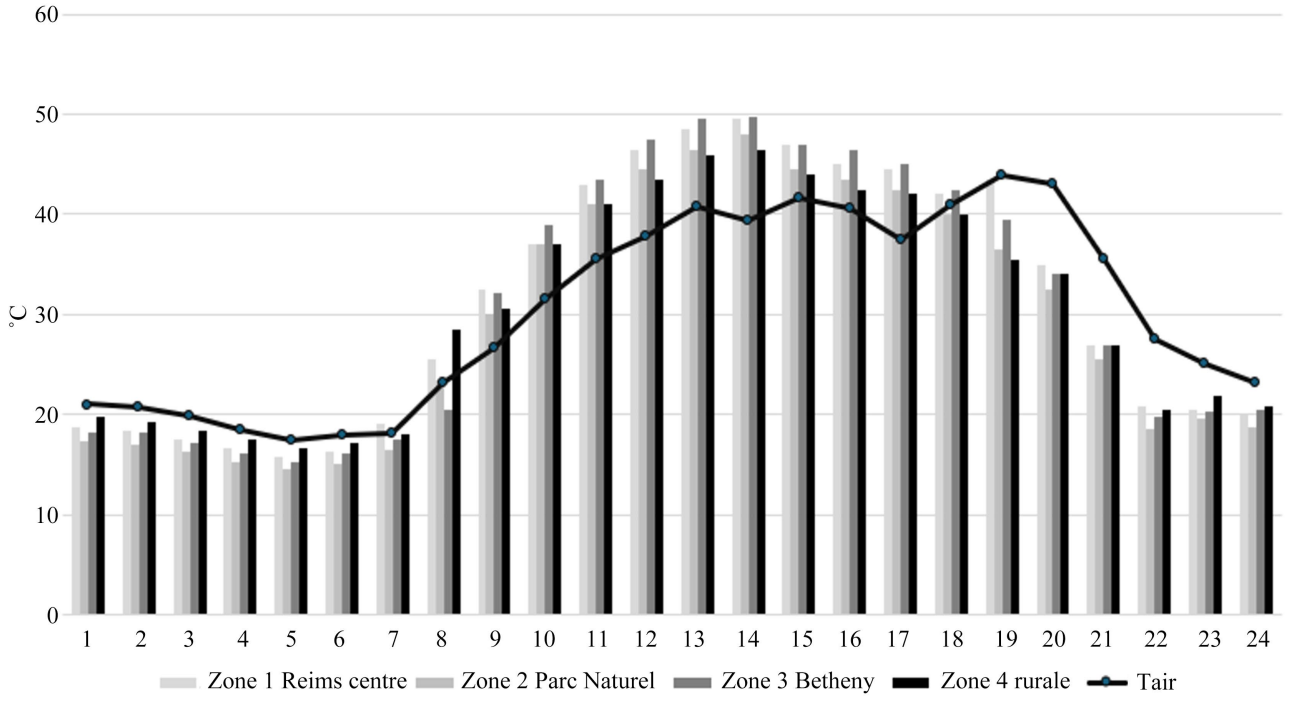

Figure 10. Analysis of the mean radiative temperature in ˚C of the study areas over 24 hours in July as a function of air temperature.

Figure 10 highlights the major influence of surface type (urban vs natural) on daytime heating. The city center accumulates more heat and releases it more slowly, thereby intensifying the urban heat island effect through elevated MRT, particularly in the late afternoon. As a result, air temperature also rises towards the end of the day, since the retained heat from buildings and paved surfaces gradually warms the surrounding atmosphere. In contrast, vegetated or rural areas respond more rapidly to changes in solar exposure and remain comparatively cooler.

For both analyzed seasons, the MRT shows strong sensitivity to air temperature in Zone 1 (Reims city center). This sensitivity is attributed to increased radiative flux exchanges in all six directions (horizontal and vertical) with the numerous surrounding urban surfaces. In contrast, MRT is significantly less affected by air temperature in the rural zone, due to the low density of reflective or emissive surfaces, which limits radiative exchanges.

The average MRT difference between the city center and the rural zone reaches 4˚C in winter (D10) and up to 5˚C in summer (D203). This is explained by variations in urban morphology and radiative properties (emissivity and albedo) specific to each zone. Furthermore,

MRT is lowest in the natural park area, conditioned by a low albedo used in the calculation and the biophysical functioning of dense vegetation. In these areas, evapotranspiration and associated latent heat fluxes strongly limit sensible heat release, thereby constraining surface temperature increases. A comprehensive assessment of urban thermal environments, however, requires integrating both surface albedo and emissivity, since albedo governs the fraction of incoming solar radiation absorbed, while emissivity determines the efficiency of longwave radiation emission. Together, these properties critically modulate surface energy balance, enabling a robust characterization and comparison of the thermal behavior of urban versus natural surfaces. In urban environments, increasing surface albedo tends to raise mean radiant temperature due to enhanced reflection of solar radiation toward pedestrians, whereas in forested environments, despite their low albedo, tree canopies reduce MRT through shading and radiative shielding [15] studies on urban albedo MRT relationships. In addition, forests, due to their low surface albedo, can exert a warming effect; however, this effect is moderated by complex interactions between biophysical and biogeochemical processes [19].

The intermediate zones (Bétheny and the rural area) display a moderated thermal response shaped by both their heterogeneous land-cover composition and their relatively open morphological structure. Lower building density and modest building heights constrain longwave radiation trapping and reduce the frequency of multiple radiative reflections, although residual built surfaces continue to contribute to localized heat storage. Street orientation, while less influential than in compact urban canyons, still modulates shortwave exposure at specific times of day. The vegetation fraction remains the primary determinant of MRT patterns: despite providing measurable evaporative cooling, the reduced canopy density in

these zones diminishes the magnitude of latent heat fluxes relative to the natural park. Conversely, the city center of Reims exhibits the highest MRT values, driven by its compact urban morphology characterized by high building density, substantial building heights, and canyon-like configurations that intensify both shortwave and longwave radiative entrapment. Minimal vegetation cover greatly restricts latent cooling, while high-inertia materials enhance heat storage and delay evening radiative dissipation. Collectively, this spatial configuration produces a clear gradient of MRT, transitioning from strong radiative attenuation in fully vegetated environments to marked radiative amplification in the dense urban core, with intermediate zones occupying a thermally transitional regime.

3) Mean radiative temperature (MRT) optimization scenarios:

The development of MRT scenarios involves integrating climate change projections and the impacts of urban development to anticipate future thermal conditions. In this study, we propose scenarios aimed at optimizing surface emissivity and albedo, drawing on emissivity data for grey body materials and satellite-derived albedo measurements in both the visible and infrared spectra.

The MRT is directly influenced by the radiative fluxes exchanged in the urban environment, namely the incoming direct solar radiation (K_{down}), the solar radiation reflected by surfaces (K_{up}), the downward atmospheric longwave radiation (L_{down}), and the upward longwave radiation emitted by materials (L_{up}). These interactions determine the net radiative load received by the human body.

The results obtained from the coupled modeling of radiative fluxes, dynamic atmospheric inputs, and surface radiative properties, along with the MRT across different material scenarios, allow for the assessment of outdoor comfort. This approach translates environmental conditions into perceived thermal and visual sensations, accounting for exposure to solar shortwave and visible radiation, atmospheric longwave radiation, and surface reflections.

This study examines the influence of surface albedo and emissivity on human thermal comfort using a fully coupled urban energy approach. While lower albedo generally increases heat absorption and raises air and skin temperatures, significantly degrading comfort, this effect does not occur for low-albedo, low-absorption surfaces such as vegetation. The results highlight that considering both albedo and emissivity in a coupled framework, along with material-specific properties, is essential for accurate assessment of urban thermal environments and their impact on human comfort.

Improving MRT can be achieved through the optimization of surface emissivity and albedo "as illustrated in **Figure 11** and **Figure 12**". Based on satellite observations, surfaces with lower albedo absorb more visible radiation from the sky, thereby reducing the temperature of both ground and vertical surfaces. This limits the emission of short- and long-wave infrared radiation and consequently contributes to lowering MRT.

Scenario 1 replaces these surfaces with dry soil and concrete, slightly increasing albedo (0.20 - 0.25) and reflecting more solar radiation. Scenario 2 investigates

light-colored concrete and glazing, with albedo values of 0.18 - 0.21, aiming to reduce surface temperatures through higher reflectivity.

The results indicate that beyond Scenario 5 (mean soil emissivity: 0.85, mean soil albedo: 0.15; mean lateral emissivity: 0.81, mean lateral albedo: 0.15), MRT drops significantly in winter, leading to potential thermal discomfort during the colder months—despite the continued decrease in MRT during summer.

Scenario 3 (mean soil emissivity: 0.89, mean soil albedo: 0.17; mean lateral emissivity: 0.85, mean lateral albedo: 0.19), as shown in Figure 14, offers a balanced solution across both winter and summer conditions. Compared to the Scenario 1 (mean soil emissivity: 0.95, mean soil albedo: 0.20; mean lateral emissivity: 0.91, mean lateral albedo: 0.25), this scenario enables an effective compromise between outdoor thermal comfort and the energy demands.

The impact of material radiative properties (albedo and emissivity) on MRT, as assessed through seven simulation scenarios compared to a reference case, demonstrates that reducing albedo leads to lower absorption of incoming visible radiation, thereby decreasing surface temperatures particularly on lateral and ground surfaces. This results in a reduction of MRT, which translates into improved thermal comfort during the summer period. However, from Scenario 5 onward, this reduction becomes problematic in winter, as MRT drops excessively, posing a risk of thermal discomfort. Scenario 3 emerges as the optimal compromise, balancing summer and winter comfort by moderately adjusting albedo and emissivity. These simulations highlight the importance of finely tuning the radiative and optical properties of urban materials to achieve seasonally balanced thermal performance.

Figure 11 below illustrates the impact of various albedo and emissivity modification scenarios on winter MRT. It shows that the more surface properties tend to reflect radiation (*i.e.*, high albedo and low emissivity), the more MRT decreases, potentially causing winter thermal discomfort. Scenarios 5 through 7 display the lowest MRT values, while Scenario 3 offers a balanced outcome slightly reducing MRT compared to the reference without inducing excessive cooling. Scenarios 1 and 2 exhibit a more moderate response: Scenario 1 produces MRT curves close to the reference, indicating that its limited adjustments in radiative properties have only a marginal cooling effect. Scenario 2, characterized by slightly higher reflectance, shows a more noticeable but still controlled MRT reduction, suggesting a modest improvement in winter radiative performance without compromising comfort. Thus, Scenario 3 appears to be the most suitable for preserving thermal comfort in urban environments during winter, while Scenarios 1 and 2 represent conservative alternatives with minimal thermal disturbance.

Figure 12 highlights the importance of optimized management of urban surface radiative properties to reduce thermal exposure during summer. Scenarios incorporating more reflective surfaces (high albedo) or surfaces with lower emissivity effectively reduce MRT by up to 10˚C on average during critical hours. Scenario 1 demonstrates a moderate but consistent reduction in MRT, reflecting the

influence of slightly more reflective and less emissive materials that attenuate daytime heating without substantially altering winter conditions. Scenario 2 further amplifies this cooling effect, as its higher-albedo surfaces generate a more pronounced decrease in MRT during peak hours; however, this enhanced mitigation begins to introduce noticeable winter cooling, which may affect thermal comfort.

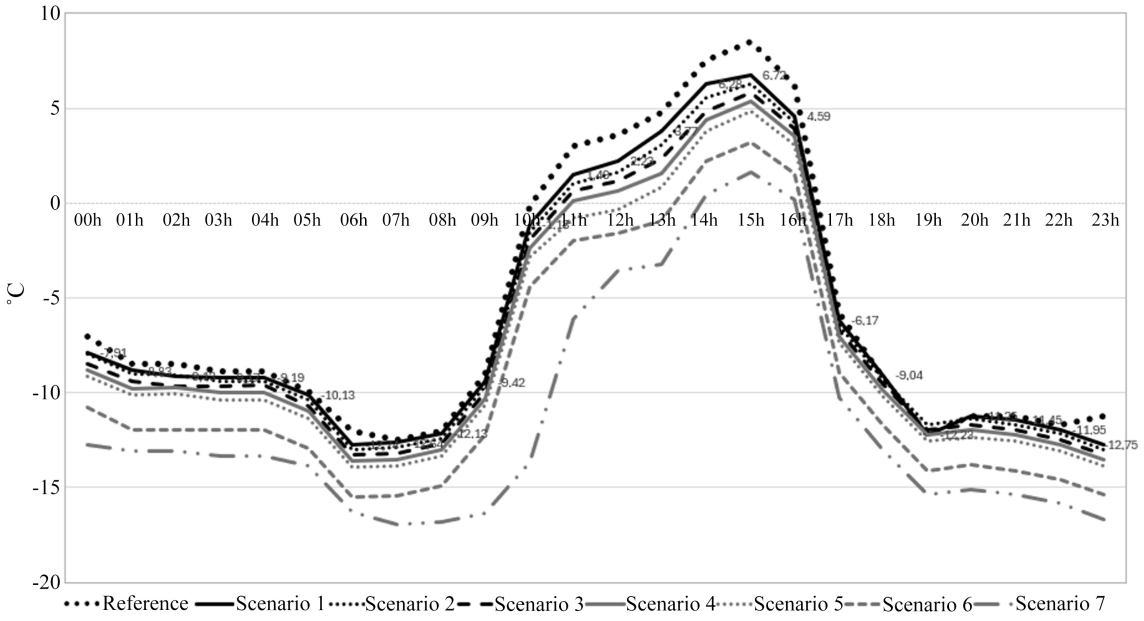

Figure 11. Evolution of mean radiative temperature as a function of different scenarios for optimizing emissivity and albedo over 24 hours in January.

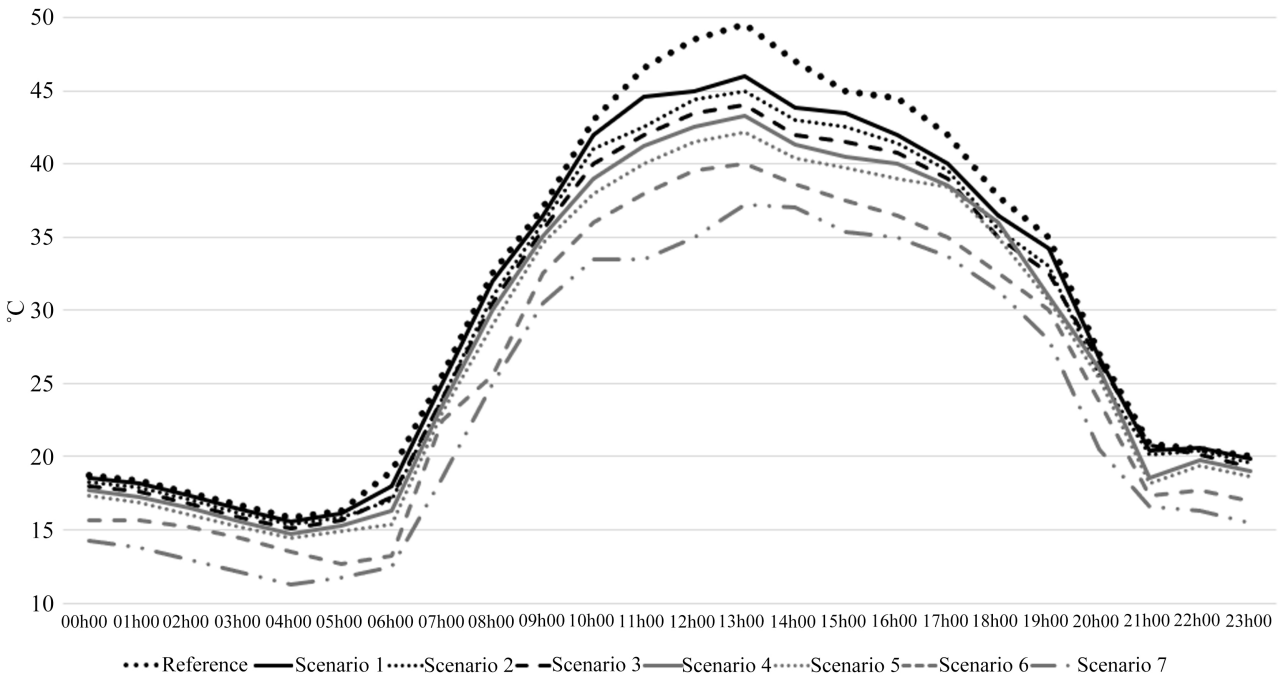

Figure 12. Evolution of mean radiative temperature as a function of different scenarios for optimizing emissivity and albedo over a 24-hour day in July.

Scenarios 4, 5, 6, and 7 intensify these radiative adjustments even further. Scenario 4 shows a significant drop in MRT, driven by highly reflective and low-emissivity surfaces that considerably suppress radiant heat loads during the warmest hours. Scenarios 5 and 6 produce even greater reductions—among the most substantial of all scenarios—highlighting the strong sensitivity of MRT to combined high albedo and reduced emissivity; yet these configurations also present a high risk of excessive winter cooling. Scenario 7, which represents the most extreme modification of surface radiative properties, yields the lowest MRT values across the day, effectively maximizing summer mitigation but clearly compromising seasonal thermal balance.

Therefore, Scenario 3 appears to offer the most balanced approach, providing effective thermal attenuation in summer while remaining compatible with winter comfort requirements.

In the context of climate warming and increasing urbanization, mitigating summer temperatures has become a priority to reduce health and energy risks associated with heatwaves. However, maintaining seasonal balance is essential, as strategies that are effective in summer (such as high-albedo surfaces) can lead to excessive cooling in winter, resulting in thermal discomfort and increased heating demand. Scenario 1, which introduces moderately reflective and emissive materials, provides a slight reduction in MRT without drastically altering the winter thermal regime, making it a conservative yet effective option. Scenario 2 amplifies this effect by employing lighter and more reflective surfaces, leading to a more pronounced decrease in MRT; however, while beneficial for summer cooling, it begins to introduce noticeable winter cooling that may compromise comfort.

Therefore, the optimal approach is to prioritize summer mitigation while adjusting radiative properties in a way that does not negatively impact winter conditions. Scenario 3 illustrates this balance particularly well, offering a seasonally coherent thermal regulation strategy that reduces summer overheating without inducing excessive winter cooling.

Figure 13 below illustrates the differences in MRT across the various scenarios compared to the reference case, with the lower section representing winter conditions and the upper section representing summer conditions.

This graph highlights the potential of urban radiative modifications (albedo, emissivity) to reduce summer mean radiant temperature and improve urban thermal comfort. It suggests that balanced scenarios (such as Scenarios 3 or 4) could provide an effective compromise between summer performance and the preservation of winter comfort.

The MRT is more sensitive to irradiation from the lower sky and ground surfaces than to lateral longwave infrared emissions from building facades, Figure 14 illustrates the sensitivity of MRT to varying values of soil and lateral surface emissivity.

This graph illustrates the importance and sensitivity of radiative emissivity in the daily thermal dynamics of urban heat islands. An increase in horizontal

ground emissivity has a more pronounced effect than that of vertical surfaces, significantly amplifying daily temperature variations, with sharper peaks during the day. This behavior is driven by factors such as orientation and exposure to solar radiation, thermal capacity and inertia, emission angle and view factor effects, as well as surface properties and roughness. These findings highlight the critical role of material selection and the radiative properties of surface coatings in thermal management strategies.

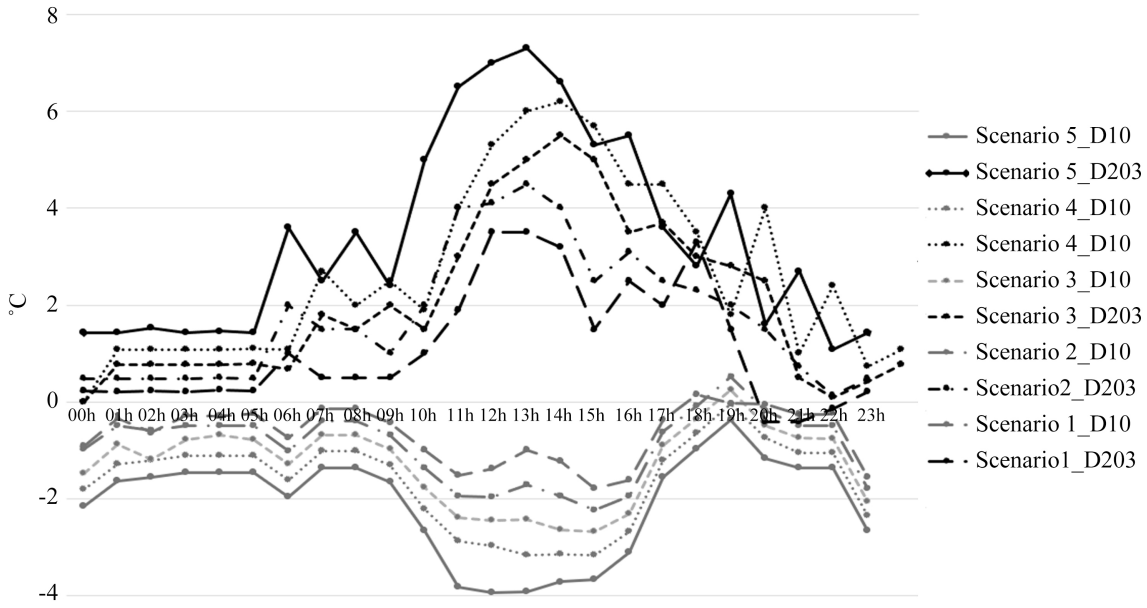

Figure 13. Difference in mean radiative temperature (MRT) between the first 5 optimization scenarios compared with the baseline.

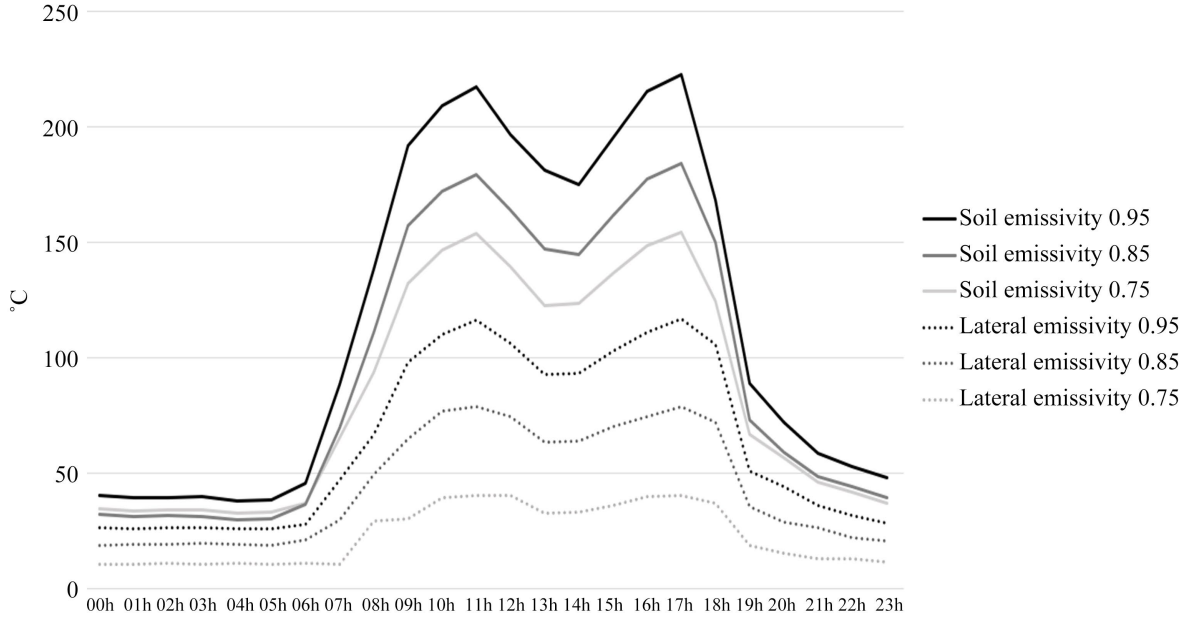

Figure 14. Analysis of the sensitivity of mean radiative temperature to variations in wall and ground emissivities in the central area of Reims.

The sensitivity analysis of ground albedo shown in Figure 15 below indicates that an increase in ground albedo leads to a rise in the Mean Radiant Temperature (MRT), particularly during the most sun-exposed hours. With the wall albedo set at 0.25 and the emissivity of both walls and ground at 0.91, more reflective surfaces return a greater amount of solar radiation toward the pedestrian space, which increases MRT, especially around midday. In the context of this sensitivity analysis, it is also important to note that a high albedo can further amplify MRT in dense urban areas where multiple reflective surfaces are present, as the combination of closely spaced buildings and reflective materials leads to repeated reflections of solar radiation within the urban canyon, thereby intensifying the radiant heat load experienced at pedestrian level; additionally, this increase in reflectivity can generate significant glare, which may reduce visual comfort and affect pedestrian perception and safety.

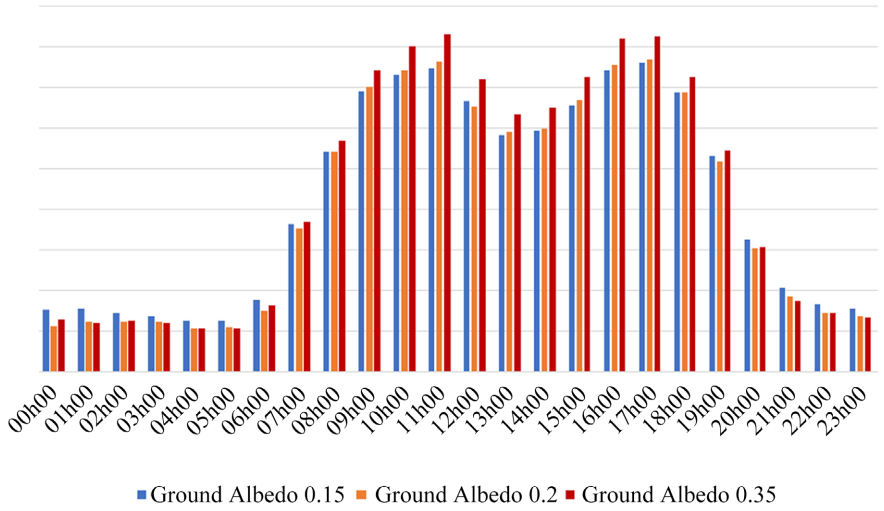

Figure 15. Sensitivity of ground albedo on the MRT in˚C in Reims city center 17 Juillet.

4. Discussion

The results highlight the importance of considering both albedo and emissivity when analyzing the radiative behavior of urban surfaces and their influence on mean radiant temperature (MRT). While many previous studies have focused primarily on the role of albedo as a strategy to mitigate urban heat islands through reflective materials, the present study demonstrates that emissivity also plays a crucial role in the urban energy balance. Indeed, surface emissivity directly affects the re-emission of absorbed thermal energy in the longwave infrared spectrum, thereby influencing surface temperature and radiative exchanges within the urban canopy.

The simulations show that increasing albedo reduces the absorption of incoming solar radiation and consequently lowers daytime MRT, confirming the effectiveness of reflective surfaces widely discussed in the literature. The results also indicate that variations in emissivity significantly influence the radiative response

of urban materials, particularly for horizontal surfaces such as the ground. Due to their direct exposure to solar radiation and their greater capacity to store heat, ground surfaces exhibit stronger sensitivity to emissivity changes, affecting both the magnitude and timing of longwave radiation release.

This behavior is governed by the spectral radiative properties of materials. In the shortwave (visible) range, surface reflection is characterized by albedo, which determines the fraction of incoming solar radiation reflected by the surface, while the remaining energy is absorbed and contributes to surface heating. The absorbed energy is subsequently re-emitted in the infrared range, where emissivity controls the efficiency of longwave radiative emission. Therefore, the balance between solar reflection (albedo), absorption, and infrared re-emission (emissivity) regulates the surface radiative response and explains the pronounced sensitivity of horizontal ground surfaces to emissivity variations.

These findings suggest that focusing exclusively on albedo may provide an incomplete understanding of urban radiative processes. A combined analysis of albedo and emissivity allows for a more comprehensive assessment of surface thermal behavior and enables the identification of optimal radiative configurations capable of reducing the Mean Radiant Temperature while maintaining a balanced thermal response throughout the diurnal cycle.

Overall, integrating both parameters into urban climate analyses provides a more robust framework for designing effective heat mitigation strategies and improving outdoor thermal comfort in dense urban environments.

5. Conclusions

Mean Radiant Temperature (MRT) is strongly controlled by surface radiative properties, particularly albedo and emissivity, whereby lower values generally reduce both shortwave absorption and longwave re-emission. Across the study domains, MRT closely follows the diurnal evolution of air temperature, although marked deviations are observed in Zone 1, where intense surface heating and direct solar exposure, especially around midday, produce significantly elevated MRT levels.

The pronounced sensitivity of ground-level surfaces to emissivity arises from combined radiative and geometric controls. Their horizontal orientation maximizes exposure to incoming solar radiation, while their higher thermal capacity enhances daytime heat storage and subsequent release. Moreover, emissivity is modulated by surface roughness, emission angles, and shape factors, which are typically more significant for ground materials, leading to enhanced hemispherical emissivity and a stronger contribution to MRT variability.

From a temporal perspective, high-albedo and low-emissivity configurations effectively reduce daytime MRT, thereby alleviating summer thermal stress. However, they may intensify nocturnal cooling, which is beneficial under hot climatic conditions but potentially detrimental during colder periods. Within dense urban fabrics, reducing MRT remains critical for mitigating urban heat island (UHI) in-

tensity and lowering cooling energy demand. In this regard, intermediate design scenarios (e.g., Scenarios 3 and 4) appear to provide a more robust compromise by moderating MRT across both diurnal phases.

The incorporation of MRT within urban heat island diagnostics offers a physically consistent basis for evaluating mitigation strategies. Optimizing surface radiative characteristics, particularly albedo and emissivity, emerges as a key lever for reducing MRT and enhancing outdoor thermal comfort. Results further demonstrate a higher MRT sensitivity to horizontal compared to vertical surfaces, underscoring the primacy of ground-level material selection over façade-oriented interventions in urban design.

Urban vegetation represents a complementary mitigation pathway through combined shading and evapotranspiration processes, which reduce net radiative load and enhance local cooling. Nevertheless, its effectiveness depends on careful spatial integration to balance shading benefits with modified heat and moisture exchanges within urban environments.

Collectively, MRT based scenarios highlight the dominant role of radiative surface exchanges in governing urban thermal regimes, providing a mechanistic framework for assessing outdoor thermal comfort under climate change and urban densification pressures.

Further spectral considerations of MRT can refine the understanding of radiative transfer processes, while greenhouse gas (GHG) forcing indirectly exacerbates urban heat accumulation by modifying atmospheric radiative balance. These coupled effects reinforce the need for integrated urban-scale mitigation strategies. Embedding optimized radiative materials into planning policies can therefore contribute to reducing MRT, attenuating UHI intensity, and supporting broader climate adaptation and emission reduction objectives.

Finally, the deployment of high-albedo surfaces at urban scale requires careful consideration of shortwave multiple reflection processes within urban canyons. Neglecting reflection absorption interactions may lead to increased pedestrian exposure to reflected radiation, elevated MRT, and potential glare effects. Consequently, the efficiency of such interventions is strongly governed by urban morphology and spatial configuration. High-reflectance materials are therefore more suitable for rooftop applications, where reflected radiation can escape to the atmosphere, whereas ground-level implementation may intensify radiative trapping and human thermal exposure.

Conflicts of Interest

The authors declare no conflicts of interest regarding the publication of this paper.

References

[1] GIEC-IPCC (2019) Réchauffement planétaire de 1,5 °C. https://www.ipcc.ch/site/assets/uploads/sites/2/2019/09/SR15_Summary_Volume_french.pdf

[2] IPCC AR6 WGII Chapter 6 (2022) Chapter 6: Cities, Settlements and Key Infrastructure. Climate Change 2022: Impacts, Adaptation and Vulnerability.

[3] Bocquier, P. (2005) World Urbanization Prospects: An Alternative to the UN Model of Projection Compatible with the Mobility Transition Theory. *Demographic Research*, **12**, 197-236. https://doi.org/10.4054/demres.2005.12.9

[4] Stewart, I.D. and Oke, T.R. (2012) Local Climate Zones for Urban Temperature Studies. *Bulletin of the American Meteorological Society*, **93**, 1879-1900. https://doi.org/10.1175/bams-d-11-00019.1

[5] Demuzere, M., Kittner, J., Martilli, A., Mills, G., Moede, C., Stewart, I.D., *et al.* (2022) A Global Map of Local Climate Zones to Support Earth System Modelling and Urban-Scale Environmental Science. *Earth System Science Data*, **14**, 3835-3873. https://doi.org/10.5194/essd-14-3835-2022

[6] Santamouris, M. (2020) Recent Progress on Urban Overheating and Heat Island Research. Integrated Assessment of the Energy, Environmental, Vulnerability and Health Impact. Synergies with the Global Climate Change. *Energy and Buildings*, **207**, Article ID: 109482. https://doi.org/10.1016/j.enbuild.2019.109482

[7] Fraisse, P. (2017) Délos: Études de morphologie urbaine I Objectifs et méthodes. *Bulletin de correspondance hellénique*, **144**, 357-371.

[8] Mirzabeigi, S. and Razkenari, M. (2022) Design Optimization of Urban Typologies: A Framework for Evaluating Building Energy Performance and Outdoor Thermal Comfort. *Sustainable Cities and Society*, **76**, Article ID: 103515. https://doi.org/10.1016/j.scs.2021.103515

[9] Acero, J.A., Koh, E.J.Y., Ruefenacht, L.A. and Norford, L.K. (2021) Modelling the Influence of High-Rise Urban Geometry on Outdoor Thermal Comfort in Singapore. *Urban Climate*, **36**, Article ID: 100775. https://doi.org/10.1016/j.uclim.2021.100775

[10] Aghamolaei, R., Fallahpour, M. and Mirzaei, P.A. (2021) Tempo-spatial Thermal Comfort Analysis of Urban Heat Island with Coupling of CFD and Building Energy Simulation. *Energy and Buildings*, **251**, Article ID: 111317. https://doi.org/10.1016/j.enbuild.2021.111317

[11] Mariani, L., Parisi, S.G., Cola, G., Lafortezza, R., Colangelo, G. and Sanesi, G. (2016) Climatological Analysis of the Mitigating Effect of Vegetation on the Urban Heat Island of Milan, Italy. *Science of the Total Environment*, **569**, 762-773. https://doi.org/10.1016/j.scitotenv.2016.06.111

[12] Santamouris, M. (2016) Cooling the Buildings—Past, Present and Future. *Energy and Buildings*, **128**, 617-638. https://doi.org/10.1016/j.enbuild.2016.07.034

[13] Watson, I.D. and Johnson, G.T. (1987) Graphical Estimation of Sky View-factors in Urban Environments. *Journal of Climatology*, **7**, 193-197. https://doi.org/10.1002/joc.3370070210

[14] Middel, A., Lukasczyk, J., Maciejewski, R., Demuzere, M. and Roth, M. (2018) Sky View Factor Footprints for Urban Climate Modeling. *Urban Climate*, **25**, 120-134. https://doi.org/10.1016/j.uclim.2018.05.004

[15] Lindberg, F., Grimmond, C.S.B., Gabey, A., Huang, B., Kent, C.W., Sun, T., *et al.* (2018) Urban Multi-Scale Environmental Predictor (UMEP): An Integrated Tool for City-Based Climate Services. *Environmental Modelling & Software*, **99**, 70-87. https://doi.org/10.1016/j.envsoft.2017.09.020

[16] Prata, A. (1996) A New Long-Wave Formula for Estimating Downward Clear-Sky Radiation at the Surface. *Quarterly Journal of the Royal Meteorological Society*, **122**, 1127-1151. https://doi.org/10.1256/smsqj.53305

[17] Robinson, D. and Stone, A. (2004) Solar Radiation Modelling in the Urban Context. *Solar Energy*, **77**, 295-309. https://doi.org/10.1016/j.solener.2004.05.010

[18] Holmer, B., Lindberg, F., Rayner, D., *et al.* (2015) How to Transform the Standing Man from a Box to a Cylinder—A Modified Methodology To calculate Mean Radiant Temperature in Field Studies and Models. http://www.meteo.fr/cic/meetings/2015/ICUC9/LongAbstracts/bph5-2-3271344_a.pdf

[19] Kirschbaum, M.U.F., Whitehead, D., Dean, S.M., Beets, P.N., Shepherd, J.D. and Ausseil, A.E. (2011) Implications of Albedo Changes Following Afforestation on the Benefits of Forests as Carbon Sinks. *Biogeosciences*, **8**, 3687-3696. https://doi.org/10.5194/bg-8-3687-2011

List of Abbreviations

- DEM—Digital Elevation Model
- DSM—Digital Surface Model
- DHM—Digital Height Model
- DTM—Digital Terrain Model
- ECT—External Comfort Temperature
- EPW—Energy Plus Weather
- ESRI—Environmental Systems Research Institute
- GHG—Greenhouse Gas
- GIS—Geographic Information System
- HD—High Definition
- IGN—Institut National de l'Information Géographique et Forestière
- IPCC—Intergovernmental Panel on Climate Change
- IWEC—International Weather for Energy Calculations
- K_{up}—Outgoing shortwave radiation
- K_{down}—Incoming shortwave radiation
- LCZ—Local Climate Zones
- L_{up}—Outgoing longwave radiation
- L_{down}—Incoming longwave radiation
- LAZ—LAS Zip (compressed LAS LiDAR file format)
- MRT—Mean Radiant Temperature
- NDSM—Normalized Digital Surface Model
- NIR—Near-Infrared
- QGIS—Quantum Geographic Information System
- RH—Relative Humidity
- SRA—Sky Radiance Approach
- SOLWEIG—Solar and LongWave Environmental Irradiance Geometry
- SVF—Sky View Factor
- Ta—Air temperature at standard height
- TMYx—Typical Meteorological Year (extended)
- UMEP—Urban Multi-scale Environmental Predictor
- WSA—White-Sky Albedo
- WSA_vis—White-Sky Albedo in the visible spectrum
- WSA_nir—White-Sky Albedo in the near-infrared spectrum